Synthetic Aperture Ultrasound imaging using GPUs (Generación de imágenes de ultrasonido por apertura sintética utilizando GPUs)

Juan Manuel Iriarte, Guillermo Cosarinsky and Jose Brizuela

***Abstract* - Ultrasound images are widely used for medical diagnosis and for Non-Destructive Testing (NDT) in the industry. Among alternative imaging methods there are the Phased Array techniques, which allow processing ultrasound signals in real time and generating focused images within certain limits. On the other hand, there are synthetic aperture techniques, commonly called SAFT, which are post-processing procedures that allow the focusing of all image points in both emission and reception. However, the use of SAFT techniques often are conditioned on industry by the high computational cost that require. This paper deals with the implementation of an algorithm for synthetic aperture imaging using a parallel processing platform. The development has been tested and validated on reference parts and nuclear industry testing pieces**.

***Index terms*: ultrasound images, industrial NDT phased array, synthetic aperture for industry.**

I. INTRODUCTION

Ultrasound images have emerged as a common technique in the field of NDT, allowing the inspection of a volume in a quantitative and qualitative way for providing the component integrity. The technique has the advantage of not generating ionizing radiation and also can be applied during component operation from one side to detect volumetric discontinuities, material characterization and life-time estimation. These features are useful, for example, in the quantitative assessment of weld cracks.

In the recent years, the Phased Array Ultrasonic Testing (PAUT) has become a widespread imaging technique, which allows steering and focusing the ultrasound beam by the electronic control of N independent array elements. The PAUT technology offers good frame rate for real-time imaging visualization (between 20 and 30 images per second), and facilitates the development of sectorial or linear scans without moving the transducer, as well as the ability to focus the beam at different points within the material (even at all depths with dynamic focusing) [1]. However, PAUT technology has its limitations, particularly when trying to assess characteristics of specular reflectors (eg., cracks and angular edges), which produce only significant reflections when the beam direction is perpendicular to the orientation of the defect [2]. Consequently, many defects cannot be properly evaluated with a single image PAUT.

A simple way to generate ultrasound images is exploring the test piece with a transducer for emitting interrogating pulses and receiving echoes, which return from the internal discontinuities (pulse-echo technique). Then, the information is reconstructed by placing the registered echoes in each transducer position on a matrix of points (image), which contains amplitude levels encoded as colors. The size of the image matrix corresponds to the region of interest (ROI). However, the use of a focused ultrasonic beam allows a good resolution only in the length of the focus range. On the other hand, if an unfocused beam is used, the resulting image would be blurred and difficult to interpret. In these situations, Synthetic Aperture Focusing Techniques (SAFT) is a good option for imaging.

The SAFT techniques were developed in the early 50`s for radar systems [3], and are widely used in medical diagnosis [4], seismic exploration [5] and NDT [6]. The lateral displacement of an unfocused source, allows to acquire signals (A-Scans) containing complete information of the component. Then, the image is generated by the coherent addition of the ultrasonic signals captured in different positions. Each point (pixel) of the SAFT image has an intensity computed according to the round-trip time of flight to the source. This proposal allows improving the resolution in the direction of movement of the source.

A. SAFT imaging method.

The process involved in the formation of a SAFT image is represented schematically in Fig. 1, assuming that ROI is located on the *xz* plane. Since the length of the transducer in the *x*-direction is comparable with the wavelength, the wavefront can be approximated as omnidirectional [7].

The pulse emitted by the transducer from the *i*-position, with coordinates (x_{iT}, z_{iT}), has a round trip to a point P of the image, with coordinates (x_P, z_P), in a time:

$$t_{iP} = \frac{2}{c}\left|\vec{r}_{iP}\right| = \frac{2}{c}\sqrt{(x_{iT} - x_P)^2 + (z_{iT} - z_P)^2} \qquad (1)$$

This work has been funded by the ANPCyT within the framework of research project PICT-2014-1768.

Iriarte Juan Manuel in now with INEND-CNEA (Comisión Nacional de Energía Atómica) as Ultrasonic researcher (iriarte@cnea.gov.ar).

Guillermo Cosarinsky is now with IAMEND-CNEA (Comisión Nacional de Energía Atómica) as Physics and researcher in Optcial NDT techniques. (gcosarinsky@cnea.gov.ar).

Jose Brizuela is now with CONICET and INEND-CNEA as main researcher in Advanced Ultrasonic Techniques. (jbrizuelasanchez@gmail.com.ar).

978-1-5090-2938-9/16/$31.00 ©2016 IEEE

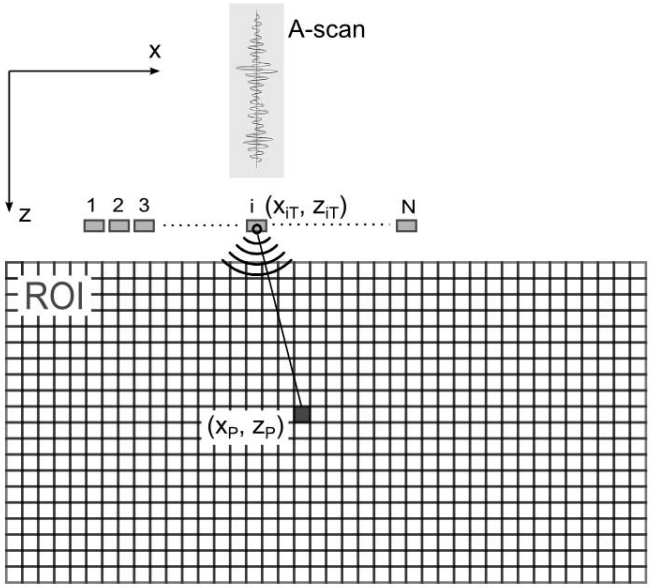

Fig 1. Simplified SAFT image procedure for reconstructing the ROI.

where $\vec{r}_{iP}$ is the vector distance from source to image point and *c* is the speed of sound in the material. The A-scan signal $a_i(t)$, which was recorded by the transducer in the *i*-position, contains echoes produced by scattering of the spherical wavefront *g(t)*. Assuming that the reflected wave detected is a scaled and delayed copy of the original pulse *g(t)*, and without considering the reflections of second and third order, then the received signal can be computed as sum over all the image pixels:

$$a_i(t) = \sum_P \eta_P g\left(t - t_{iP}\right) \tag{2}$$

Where η_P is the attenuation coefficient for each pixel *P* of the ROI. Then, the intensity of the pixel *P* is obtained by considering the information captured by the transducer from the *N* positions used for synthetic aperture. The intensity is computed as:

$$I_P = \left| \sum_{i=1}^{N} \omega_i A_i\left(t_{iP}\right) \right| \tag{3}$$

where ω_i is an apodization factor that can be used to reduce sidelobes [8]. On the other hand, $A_i(t)$ is the analytical representation of the $a_i(t)$ signal received by the transducer at the *i*-position obtained by applying the Hilbert transform $H(\bullet)$:

$$A_i(t) = a_i(t) + j \cdot H\left(a_i(t)\right) \tag{4}$$

The absolute value in (3) is for the envelope extraction of the synthesized signal, which allows visualizing the ultrasound images in video mode.

II. MATERIALS AND METHODS

Implementation of SAFT technique was performed using a phased array system of 32 active channels multiplexed to 128 (DASEL SL, Spain), using an array of 128 transducer elements, and center frequency of 5 MHz. The spacing between the centers elements is 0.5 mm (*pitch value*). Due to the small-size elements, the transducers can be considered as punctual sources of omnidirectional waves. To emulate the synthetic aperture, each element was sequentially activated until to cover the entire array.

The images have been processed using an Intel Core i7-3770 processor @ 3.4GHz 8-core 64-bit with 8GB of RAM, running Matlab® with a script that implements (3). Python environment was used to run two kernels which compute (3), one developed in C, and another written in OpenCL to control a GPU parallel processors platform (Asus Strix-R9 390X-DC3 8GB of RAM).

A. Test piece # 1

A piece with five copper wires of 0.5 mm diameter located at different depths and distributed following a slope of 30° was used first (Fig. 2). It was immersed in degassed water, which acts as a coupling material. The array was located at 25 mm from the first reflector. The ROI generated is 1.8 Mpixels, large enough to represent all reference reflectors.

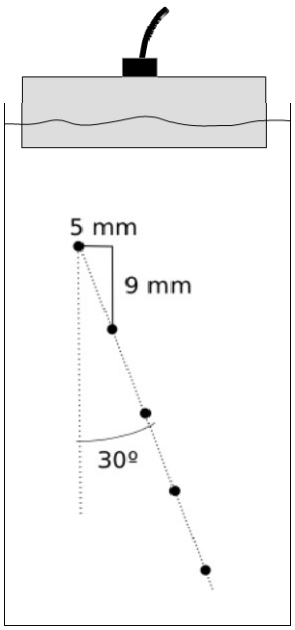

Fig 2. Arrangement for the test piece #1 and the spaces related to their reflectors.

B. Test Piece # 2

This test piece is an aluminum block of 36mm thickness, which contains a machined notch EDM. The reference reflector is perpendicular to the surface of 18 mm height and 0.25 mm wide. The array is in contact with the test piece and located on the tip of the notch (Fig. 3).

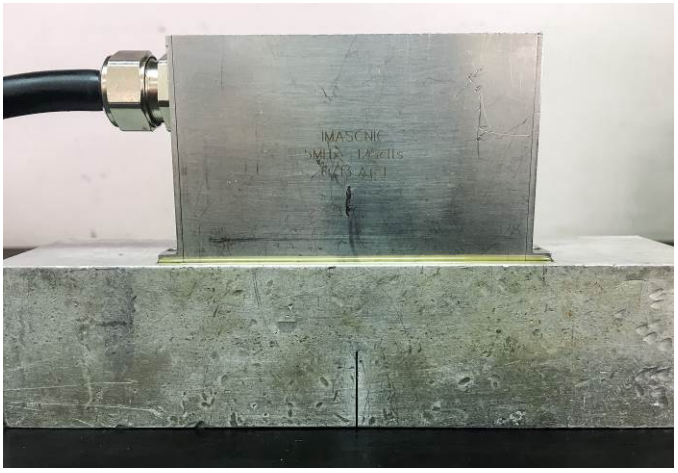

Fig 3. Conditions for testing reference block #2.

C. *Test piece # 3*

Finally an austenitic steel reference nuclear block of 26 mm thickness was used, which includes two side drilled holes of 3 mm diameter located at different depths (their centers are located at 16 mm and 8 mm from the surface and spaced at 50 mm between their centers). The test was performed in contact (Fig. 4).

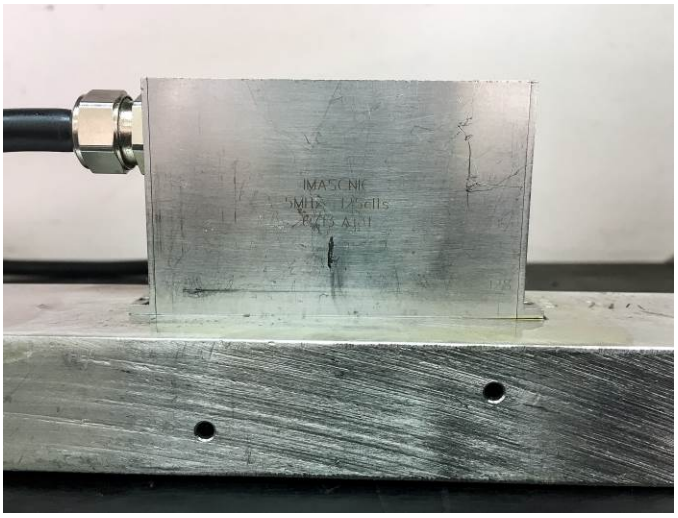

Fig 4. Conditions for testing reference block #3.

III. RESULTS

The following images have been generated using GPU. However, the results are independent of the selected processing platform.

The acquisition data of the test piece # 1 was performed in an immersion media using a sampling frequency of 20 MHz. In the B-scan image formed with the raw data can be observed the effect of emitting with small-size elements. Because of the spherical wavefront, reflectors can be seen as hyperboles. The image colors are in logarithmic scale over a dynamic range between -40 and 0 dB (Fig. 5). It is also possible to see that the data acquired in the response of each array element is different, some of them are more sensitive than others. Moreover, they have different noise levels (some columns are more intense than others).

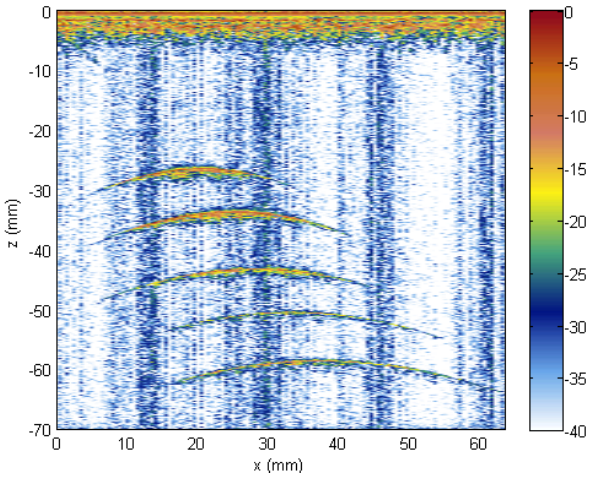

Fig 5. Test piece #1 original B-scan image. Reflectors are observed as hyperbolas. Image scale range in decibels.

After beamforming the image of 1400 x 1280 pixels (height and width) by equation (3), it can be seen a significant improvement in the signal-to-noise ratio (SNR) compared to the original information. Moreover, it is observed that higher resolution of the reflectors have been achieved, so a quantitative analysis of the information can be provide (Fig. 6). The sidelobes and grating lobes formed due to reflectors which are closest to the array are present too. These artifacts in the image are typical of this imaging technique that uses only one element as a receiver [9 -10].

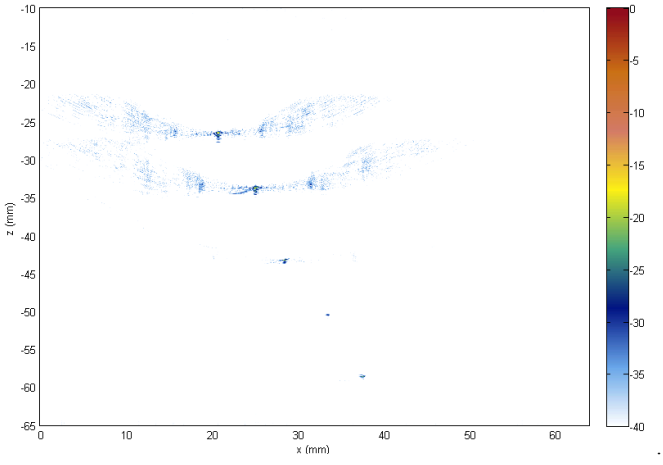

Fig 6. SAFT image composed for test piece #1. Again, image scale range is in decibels.

In the case of test piece # 2 the results obtained are not good enough if PAUT technique is applied. For example, when using a linear scan with 32 active elements aperture and

dynamic beam focusing perpendicular to the surface, it is possible to see the notch tip diffraction (Fig. 7). The image displayed on linear scale has very good SNR. Indeed, using 32 elements to generate acoustic beam allows transferring greater energy to the medium than using a single one. Using the full width at half maximum (FWHM) to evaluate the tip diffraction, the notch width measured (1.5 mm) is larger than the real width (0.25mm). After composing the image using (3) with a sampling frequency of 40 MHz, the tip diffraction can be assessed more effectively due to a better resolution. In this case the width obtained from the notch is 0.5 mm (Fig. 9), which means a significant improvement over PAUT conventional techniques. The sizing error is associated with the wavelength and not to the imaging technique.

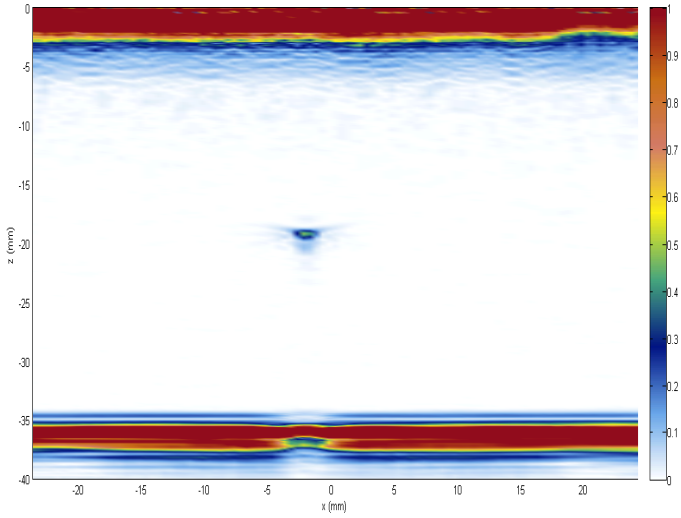

Fig 7. PAUT image from test piece #2. The notch tip is in the center.

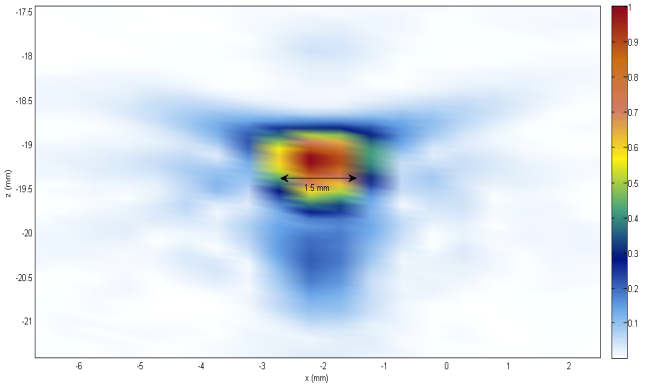

Fig 8. Zoom to the notch tip diffraction associated to test piece #2.

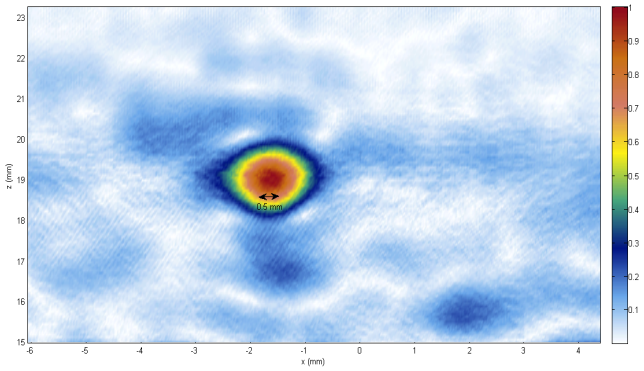

Fig 9. Zoom to the notch tip diffraction associated to test piece #2 processed with SAFT.

Although the tip diffraction is obtained with higher resolution than PAUT technique, SAFT image has a lower SNR. In fact, this is because the ROI is reconstructed using smaller transducers, which provide less energy than the 32-elements aperture used to obtain the PAUT image.

Finally, the test piece # 3, which is made of austenitic steel, has greater attenuation for the ultrasonic signal than the other cases. This effect is significant when the array elements have a small area (in this case 0.4 mm width and 10 mm height). Data acquisition was performed at 40 MHz. The ROI defined in a space of 30 mm height by 64 mm width is reconstructed using an image of 1200 x 1800 pixels (height and width). Although the indications of the reflectors are weak, they are placed at the correct position (Fig. 10). The reflector positioned at 16 mm from the surface can be clearly distinguished, is merged with the dead zone of the input pulse because it is very close to the surface. Moreover, it can be verified that the space between both reflectors is 50 mm. The image color scale is logarithmic with a dynamic range between -45 and 0 dB.

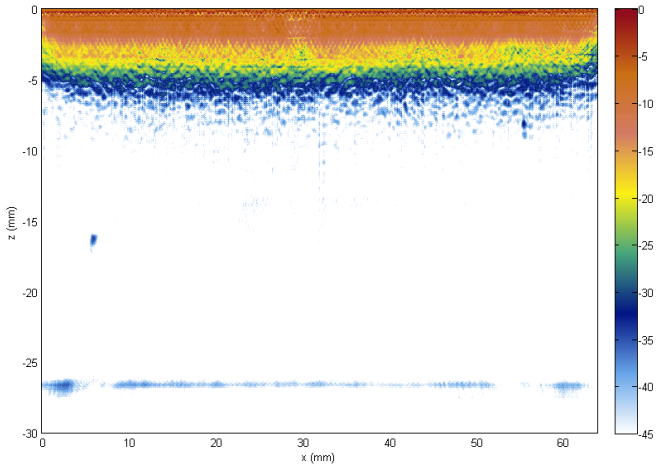

Fig 10. Image SAFT processed for test piece #3.

A. Processing

In order to analyze the computing time used by each kernel, images acquisitions in water are taken as reference. Images are captured in this medium using a transducer frequency f = 5MHz, which is sampled at a frequency fs = 40 MHz. This is the worst case for testing. In fact, the propagation speed in water is much slower than in metals (c = 1.48 mm/us), resulting in a wavelength $\lambda = c / f \approx 0.3$ mm. Thus 8 points are obtained in a wave cycle in water acquisitions cases. Therefore, the number of recorded samples is high and calculating (3) requires addressing samples within large memory buffers. The reference image has a size of 1400 x 1280 pixels, which represents a ROI of 60 x 64 mm.

The Matlab® script requires 41.18 seconds to generate the output image. On the other hand, the kernels in C and OpenCL demand 11.31 and 0.016 seconds respectively, to generate the same output image (Table 1). These times do not take into account the times involved in loading the input data to memory and writing the results to disk, it is only considered the performance of the code that computes (3). This results show that the use of a parallel platform is well suited for such applications. The C code performance is good within certain limits. For image sizes greater than about 1.8 Mpixels, the processing time increases because of problems with memory management. Finally, the use of Matlab® can provide a method for fast prototyping of image composition algorithms. However when large images are composed, the processing time becomes higher and there might be problems with memory dump.

TABLE I. PROCESSING TIMES

Image size	**Kernel**		
	Matlab®	***Python+C***	***Python+OpenCl***
1400 x 1280 pixels	41.18 s	11.31 s	0.016 s

IV. CONCLUSIONS

In this paper the development of a simple synthetic aperture imaging (SAFT) algorithm was addressed. This algorithm was tested over different experiments with positive results. The postprocessing technique based on synthetic aperture produces images of high resolution, with a relatively simple mechanism. However, the use of a single array element in emitting stage has some limitations, the most significant are formation of grating lobes and low SNR. These problems can be solved using virtual sources [13] for increasing the acoustic energy or the Total Focusing Method (TFM), which combines the emission of one array element with simultaneous reception of all the array elements. In this way a better SNR is achieved, the sidelobes and grating lobes are reduced and the probability of detection of defects increases regardless of their orientation. Another possibility that was not addressed in this paper is imaging with material interface that produces refraction and so increases the complexity of the calculations. In that case, processing times are considerably increased. For example, the generation of a 120x80 pixels image with a random interface can reach more than 1 hour processing with a Matlab® script running on a computer with two quad-core 3 GHz processors [14]. Therefore, the development of GPU processing ensures further progress with this imaging technique on more demanding scenarios than those presented in this paper.

ACKNOWLEDGMENT

This work has been funded by the ANPCyT within the framework of research project PICT-2014-1768.

REFERENCES

[1] C. Fritsch, M. Parrilla, A. Ibáñez, R.C. Giacchetta, and O. Martínez, "The Progressive Focusing Correction Technique for Ultrasound Beamforming". IEEE Trans. UFFC, vol. 53 (10), pp. 1820-1830, 2006.

[2] T. Armitt, "Phased arrays not the answer to every application", 9th European NDT Conference – ECNDT 2006 Proceedings, We.3.1.3. Berlín, Alemania. Septiembre 2006.

[3] N. A. Goodman and J. M. Stiles, "The information content of multiple receive aperture sar systems," Proc. of IEEE Geoscience and Remote Sensing Symposium, vol. 4, pp. 1614–1616, 2001.

[4] H. Yao, "Synthetic Aperture Methods for Medical Ultrasonic Imaging", Ph.D. Tesis, Ed. University of Oslo, 1997.

[5] G. Wang K. Gu and J. Li, "Migration based SAR imaging for ground penetrating radar systems", IEEE Proc. Radar Sonar Navig., vol. 151(5), pp. 317-325, 2004.

[6] P. D. Corl, P. M. Grant, and G. S. Kino, "A digital synthetic focus acoustic imaging system for nde", IEEE Ultrasonic Symposium, pp. 263–268, 1978.

[7] C. Frazier and W. O'Brien, "Synthetic aperture techniques with a virtual source element". IEEE Trans. on UFFC, vol. 45 (1), pp. 196-207, 1998.

[8] F. Lingvall, T. Olofsson, and T. Stepinski, "Synthetic aperture imaging using sources with finite aperture: Deconvolution of the spatial impulse response", J. Acoust. Soc. Am. Vol 114 (1), pp. 225 – 234, 2003.

[9] C. J. Martín, O. Martínez, L. G. Ullate, A. Octavio, G. Godoy, "Reduction of Grating Lobes in SAFT Images", Proc. IEEE Ultrason. Symp. pp. 721-724, 2008.

[10] O. T. von Ramm and S. W, Smith, "Beam steering with linear arrays". Trans. IEEE on Biomedical Eng., vol. 30(8), pp. 438-452, 1983.

[11] C. Holmes, B. Drinkwater, P. Wilcox, "Post-processing of the full matrix of ultrasonic transmit–receive array data for non-destructive evaluation," NDT & E International, 38, 8, pp. 701-711, 2005.

[12] J. Zhang, B. W. Drinkwater, P. D. Wilcox, A. J. Hunter, "Defect detection using ultrasonic arrays: The multi-mode total focusing method," NDT & E International, 43, 2, pp. 123-133, 2010.

[13] J. Brizuela, P. Katchadjian, C. Desimone, A. Garcia, "Virtual ultrasound sources for inspecting nuclear components of coarse-grained structure", AIP Conference Proceedings, vol. 1581 (1), pp. 1053-1060, 2014.

[14] M. Suttcliffe, M. Weston, B. Dutton and I. Cooper, "Real-time full matrix capture with auto-focusing of known geometry through dual layered media", NDT Conf. of BINDT, Daventry, Reino Unido, 2012.